ANTIOXIDANTS & REDOX SIGNALING
Volume 14, Number 1, 2011

DOI: 10.1089/ars.2010.3112

Interlocking Disulfides in Circular Proteins: Toward Efficient Oxidative Folding of Cyclotides

Teshome Leta Aboye,[1,2,*] Richard J. Clark,[1,3,*] Robert Burman,[1] Marta Bajona Roig,[1] David J. Craik,[3] and Ulf Göransson[1]

Abstract

Cyclotides are ultrastable plant proteins characterized by the presence of a cyclic amide backbone and three disulfide bonds that form a cystine knot. Because of their extreme stability, there has been significant interest in developing these molecules as a drug design scaffold. For this potential to be realized, efficient methods for the synthesis and oxidative folding of cyclotides need to be developed, yet we currently have only a basic understanding of the folding mechanism and the factors influencing this process. In this study, we determine the major factors influencing oxidative folding of the different subfamilies of cyclotides. The folding of all the cyclotides examined was heavily influenced by the concentration of redox reagents, with the folding rate and final yield of the native isomer greatly enhanced by high concentrations of oxidized glutathione. Addition of hydrophobic solvents to the buffer also enhanced the folding rates and appeared to alter the folding pathway. Significant deamidation and isoaspartate formation were seen when oxidation conditions were conducive to slow folding. The identification of factors that influence the folding and degradation pathways of cyclotides will facilitate the development of folding screens and optimized conditions for producing cyclotides and grafted analogs as stable peptide-based therapeutics. *Antioxid. Redox Signal.* 14, 77–86.

Introduction

The cyclotides (6) are a remarkable family of plant proteins that are characterized by a head-to-tail peptide backbone and six conserved cysteine residues that are paired to form a knotted network of three disulfide bonds. The combination of the circular peptide backbone and the tightly knotted disulfide bonds defines the cyclic cystine knot (CCK) motif. It is this feature that makes the cyclotides exceptionally stable: they are resistant to thermal unfolding, chemical denaturants, and proteolytic degradation and their use in native medicine as a uterotonic tea suggests that they are very stable in biological systems (19). This inherent stability makes the cyclotides an attractive scaffold for the design of peptide-based therapeutics (8).

Over 140 cyclotides containing between 28 and 37 amino acids have been reported to date (7, 45); example structures and sequences are shown in Figure 1. The backbone segments between the conserved cysteine residues, referred to as loops, have varying levels of sequence diversity as illustrated in Figure 1B. Loops 1 and 4 are highly conserved across all the cyclotides and together with two disulfide bonds they make a ring that is penetrated by the third disulfide to form the cystine knot. Loop 6 has recently been identified as the point of cyclization in the biosynthesis of the cyclotides and has a highly conserved asparagine/aspartic acid residue that has been recently shown to be critical in the processing of the cyclotide precursor protein by an asparagine endopeptidase (15, 35). The remaining loops (2, 3, and 5) are more variable in size and composition, but several residues are still highly conserved. Based on the presence or absence of a *cis*-Pro residue in loop 5 the cyclotides have been divided broadly into two subfamilies, namely the Möbius and bracelet, respectively.

The cyclotides exhibit a diverse range of biological activities. These include uterotonic (18), anti-HIV (22, 25, 45), hemolytic (13, 36, 42), antimicrobial (42), antifouling (17), antitumor (30, 40), and cardiotoxic activities (18), as well as inhibition of trypsin (23) and neurotensin binding (48). In addition, they exhibit insecticidal, nematocidal, and molluscidal properties and it is believed that the natural role of cyclotides in plants is as a defense against predation (1, 26, 27, 33). Many of

[1]Division of Pharmacognosy, Department of Medicinal Chemistry, Biomedical Centre, Uppsala University, Uppsala, Sweden.
[2]Department of Pharmaceutical Chemistry, School of Pharmacy, Addis Ababa University, Addis Ababa, Ethiopia.
[3]Institute for Molecular Bioscience, The University of Queensland, Brisbane, Australia.
*These two authors contributed equally to this work.

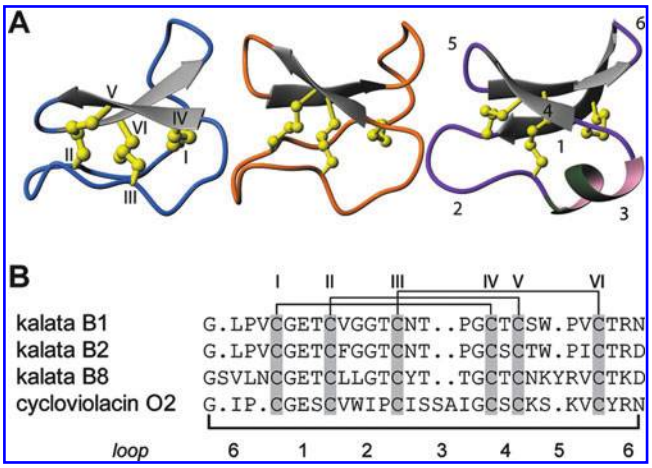

FIG. 1. Structures and sequences of cyclotides used in the present study. (**A**) Three-dimensional structures of prototypes for all three subfamilies: the Möbius kalata B1 to the left, the hybrid kalata B8 in the middle, and the bracelet cyclotide cycloviolacin O2 to the right (protein data bank codes 1nb1, 2b38, and 2knm, respectively). Note the cyclic backbones, and the disulfide bonds forming the cystine knot (cysteines are shown in yellow ball and stick format). The arrangement of cystines is shown with Roman numerals: CysI is connected to CysIV, CysII to CysV, and CysIII to CysVI. These features are conserved in all subfamilies. (**B**) Sequences of the four cyclotides used in the present study. The alignment highlights some of the differences between the subfamilies including the larger size of loop 3 in the bracelet family that forms a helix; and loop 5 that contains the *cis*-Pro bond that defines the Möbius subfamily, or the cluster of positively charged amino acids found in bracelets in particular. (For interpretation of the references to color in this figure legend, the reader is referred to the web version of this article at www.liebertonline.com/ars).

these biological activities are believed to be a result of cyclotides interacting with biological membranes (28, 39, 46).

A number of three-dimensional structures of cyclotides have been determined using nuclear magnetic resonance, including kalata B1 and B2 (27, 34), cycloviolacin O1 (34), circulins A and B (12), palicourein (2), tricyclon A (31), and cycloviolacin O2 (16), and the X-ray structure of varv F was recently reported (47). The conserved structural elements of the cyclotides include a β-hairpin that is part of a triple-stranded β-sheet formed by loops 4, 5, and 6. The third strand (*i.e.*, the one additional to the two strands of the β-hairpin) is distorted from ideal geometry and contains a β-bulge. In addition, the bracelet cyclotides have a short section of helical structure in loop 3.

A predominant feature of the cyclotides is the relatively large number of hydrophobic residues that are exposed on localized regions of the protein surface. In the Möbius cyclotides, such as kalata B1, the large hydrophobic patch is formed predominantly by the residues of loops 5 and 6. In contrast, the hydrophobic patch present in the bracelet cyclotides is comprised of residues from loops 2 and 3. The hydrophobic patch of the cyclotides is thought to have a major influence on the folding of these peptides. Consistent with this proposal, it has been shown that the addition of hydrophobic solvent and detergents to the folding buffer *in vitro* significantly improves the yield of correctly folded cyclotides (13, 29).

The relatively small size of the cyclotides ($\sim$30 amino acids) makes them amenable to chemical synthesis using solid-phase methodologies. This facilitates the production of some cyclotides that could otherwise only be isolated from natural sources in small quantities, thus allowing their characterization. In addition, chemical synthesis can be used to probe the structure/activity relationships of the cyclotides and also opens the possibility of using them as a molecular scaffold for drug design. The general methodology for synthesizing cyclotides (4, 13, 29, 44) utilizes a solid-phase approach to assemble the peptide chain followed by backbone cyclization *via* an intramolecular native chemical ligation reaction (14, 42). The ligation reaction occurs in conjunction with the oxidative folding of the peptide to form the cystine knot. The folding conditions utilized during this step are critical in forming the correct disulfide connectivity and hence the CCK motif.

There have been several studies investigating the oxidative folding pathways of cyclotides *in vitro* and the influence of the cyclic backbone on these processes. Folding studies on the prototypical Möbius cyclotide, kalata B1, have found that it can be successfully folded in aqueous buffer containing a hydrophobic cosolvent (isopropanol, iPrOH) and disulfide shuffling reagent (reduced glutathione [GSH]) (13). The folding pathway is dominated by a two-disulfide species that possesses the native CysII-CysV and CysIII-CysVI bonds (9, 10). Interestingly, this species is not the direct precursor of the native three-disulfide native peptide and the glutathione in the buffer is required to reshuffle this two-disulfide species to ultimately form the native peptide. To this date, the direct two-disulfide precursor to kalata B1 is not known. The *in vitro* folding of bracelet cyclotides has been only recently achieved, as previously the conditions typically used for Möbius cyclotides resulted in aggregated and insoluble peptide (29). A comprehensive study of the effect of temperature, salt concentration, cosolvents, detergents, and shuffling reagents on the folding of the bracelet cyclotide cycloviolacin O2 resulted in a buffer system that results in the native peptide fold as the major product. Interestingly, the folding of bracelet cyclotides appears to be dominated by nonnative three-disulfide species, with the formation of the CysI-CysII, CysIII-CysIV, and CysV-CysVI isomer as a major energetic trap (29).

In the present study, we describe a comprehensive study of the *in vitro* folding pathways of the two major subfamilies of cyclotides, Möbius and bracelet, and describe the similarities and differences between the pathways in a range of buffer conditions, highlighting the major intermediates accumulating for both families under the experimental conditions being employed. An understanding of the mechanisms of cyclotide folding and the effects of buffers on the formation of the native isomer is of great importance in the development and exploitation of cyclotides and the CCK motif in drug design.

Materials and Methods

Isolation and reduction of cyclotides

The native Möbius cyclotides, kalata B1 and B2, and the hybrid cyclotide (*i.e.*, part Möbius, part bracelet), kalata B8, were isolated from *Oldenlandia affinis*, whereas the bracelet cyclotide cycloviolacin O2 was isolated from *Viola odorata* as described previously (24, 32). In short, plant materials were extracted using dichloromethane/methanol (1/1, v/v) or ethanol/water (1/1, v/v). The extracts were subjected to

liquid–liquid extraction and concentrated *in vacuo* before solid-phase extraction on C18 support. Pure cyclotides (>95%) were then isolated using reverse-phase high-performance liquid chromatography (HPLC).

After freeze drying, peptides were dissolved (1 mg/ml) and disulfide bonds were reduced using 1,4-dithiothreitol (3 mg), guanidine (6 *M*), and Tris-HCl (0.25 *M*, pH 8.5) containing ethylenediaminetetraacetic acid (EDTA; 1 m*M*) at 37°C for 2 h. Then, 2 ml of this solution was injected and purified by reverse-phase HPLC at a flow rate of 1 ml/min, using a mixture of 5% B (60% AcN in 0.1% trifluoroacetic acid [TFA]) in A (10% AcN in 0.1% TFA) for 8.5 min to equilibrate the column, followed by a linear gradient of 5%–70% B in A for 44.5 min and a cleaning phase of 100% B for 4.5 min. Fractions were collected and analyzed using electrospray mass spectrometry (MS), and fractions containing reduced peptide were pooled and freeze-dried. Peptides were then redissolved in eluent A to a concentration of 0.3 m*M* from which 100 μl of solution was aliqouted into Eppendorf tubes, freeze-dried, and used for further experiments.

Oxidative folding

To analyze the kinetics of folding under different experimental conditions, reduced peptides were dissolved in the appropriate solvent (iPrOH or water) followed by the immediate addition of reagents required for each experiment to make a peptide concentration of 0.3 m*M* in water or 0.25 m*M* in 50% (v/v) aqueous (aq.) iPrOH or 20% (v/v) aq. dimethyl sulfoxide (DMSO) at 21°C.

The effects of reducing agents on folding kinetics were analyzed in 0.1 *M* NH_4HCO_3 (pH 8.5), in 0.1 *M* NH_4HCO_3 (pH 8.5) containing 50% (v/v) iPrOH and the following concentrations of GSH/oxidized glutathione (GSSG), 2/0, 2/0.4, 2/1, and 2/2 m*M*, in 20% (v/v) DMSO in water, and in 0.1 *M* Tris-HCl (pH 8.5) containing 1 m*M* EDTA, 6% Brij 35, 35% DMSO, 2 m*M* cystamine, and 2 m*M* GSH.

After addition of folding reagents, samples were flushed with N_2, sealed, and incubated at 21°C. For each experiment, an aliquot of 10 μl of solution was removed at the time intervals 2 min, 30 min, 1 h, 2 h, 4 h, 6 h, 10 h, 24 h, and 72 h from the reaction mixture and quenched by adding to 90 μl of *N*-ethylmaleimide (NEM) (60 m*M* in 0.2 *M* citrate buffer, pH 3).

Samples from folding experiments were analyzed with liquid chromatography (LC)-MS, using a Shimadzu LC10 HPLC system connected to a Thermo-Finnigan LCQ electrospray ion trap MS. The capillary temperature was set at 220°C and the spray voltage at 4.5 kV. Separation was done using a Water Symmetry C18 column (150×2.1 mm inner diameter (i.d.), 5 μm, 300 Å) at a flow rate of 0.3 ml/min and by using the following standard gradient: 5% B in A (using formic acid, FA, instead of TFA) for 2 min to equilibrate the column, followed by 5%–30% B in A for 2 min, a linear gradient of 30%–65% B in A for 21 min, 65%–100% B in A in 2 min, and a washing step of 100% B in A for 2 min. A volume of 20 μl of the trapped sample was injected.

Different peak areas obtained after LC-MS analysis were used as a layout for integration of the peaks. The areas under the curve in 4 mass unit wide windows were calculated, centered at the doubly charged ions $[(M+2H)^{2+}]$ of each peptide species (peptide with native disulfides [N], peptide containing three disulfide bonds [3SS], peptide containing two disulfide bonds [2SS], peptide containing one disulfide bond [1SS], and reduced peptide [R], respectively) of kalata B1 (1447.6, 1573.9, 1699.3, 1826.2), kalata B2 (1479.2, 1605.4, 1731.0, 1862.1), and cycloviolacin O2 (1572.1, 1698.0, 1821.4, 1846.4), and the triply charged $[(M+3H)^{3+}]$ ions of kalata B8 (1097.2, 1181.3, 1264.7, 1348.9) were integrated. Then the percentage represented by each subset was calculated from the areas under the curve values for each experimental condition and at each sampling time point (2 min, 30 min, 1 h, 2 h, 4 h, 6 h, 10 h, 24 h, and 72 h). Graphs were constructed using the quantities of each species (expressed in percentage). All graphs are shown in Supplemental Figures 1–5 (*see* www.liebertonline.com/ars).

Results

The main objective of the present study was to gain deeper insights into the external factors that influence oxidative folding of cyclotides. To this end, we systematically mapped the oxidative folding of selected members of each cyclotide subfamily in a standardized set of folding conditions and compared the final yield of native peptide, folding kinetics, and the accumulation of nonnative isoforms.

Four cyclotides were chosen to represent the two main subfamilies: besides kalata B1, which is the most well-studied cyclotide and the prototype for the Möbius subfamily, kalata B2 was included for comparison within the Möbius subfamily, together with prototypes for the bracelet and the growing Möbius/bracelet hybrid subfamilies in the form of cycloviolacin O2 and kalata B8, respectively. These peptides were all isolated from cyclotide-containing plants, the three disulfide bonds were then reduced, and the fully reduced species were isolated. Aliquots of the reduced material were then subjected to oxidative refolding at the different folding conditions. The reaction mixture was sampled during the folding process, and the progress was monitored using LC-MS.

To monitor the progress of oxidative folding, which is the formation of disulfide bonds to the native connectivity and structure, is an analytical challenge, even with the combination of LC and MS. Ongoing folding processes and reshuffling of disulfide bonds even after sampling, highly similar overall folds and structures, and the need to distinguish between ions of doubly and triply charged disulfide species with relatively small mass differences in peptides of molecular weights of ~3000 (the corresponding mass shifts for one, two, or three disulfides bonds are 2, 4, or 6 mass units) with overlapping isotopic envelopes are some of the main difficulties that need to be addressed. To circumvent these problems in the present study, we used a strategy of capping free thiols at low pH using NEM to quench disulfide reshuffling and to introduce a mass difference between disulfide species that are fully reduced or containing one, two, or three disulfide bonds as multiples of the molecular weight of NEM (125 g/mol). Then, the fully reduced peptide (R) accumulates 750 mass units (6×NEM), one disulfide species (1SS) 500 mass units (4×NEM), and two disulfide species (2SS) 250 mass units (2×NEM), whereas no additional mass is conferred to the three-disulfide species (3SS), of which the native peptide (N) is one. These folding species include in total 76 individual species (R, 15×1SS, 45×2SS, 15×3SS including N), which all are treated as subsets with the exception of the native peptide. N was

distinguished from the 3SS subset by means of its retention time and comparisons with native peptides isolated from plants. The ability to distinguish between native and nonnative 3SS disulfides species is important, as one of the specific aims of the present study was to evaluate the different folding systems in terms of final yield.

The standard buffer systems for cyclotide folding are based on the early work by Daly *et al.* (13), in which 0.1 *M* ammonium bicarbonate and 1 m*M* GSH in water was successfully used for folding of the prototypic cyclotide kalata B1. In that study it was also found that the folding efficiency of that Möbius cyclotide was improved in the presence of iPrOH (50%), which was hypothesized to stabilize the hydrophobic surface of the peptide. Therefore, it was logical to include these two buffer systems in the present study as bases for a systematic survey.

Using these two folding systems (0.1 *M* NH_4HCO_3, with and without iPrOH) and kalata B1 as model peptide, we first focused on the influence of redox agents, particularly on folding kinetics and final yield. The concentration of GSH was set at 2 m*M*, and four different concentrations of GSSG were used: 0, 0.4, 1, and 2 m*M*. All experiments were done under N_2 to avoid air oxidation. Under all conditions, 1SS and 2SS intermediates were observed as the folding reaction proceeded, which can be seen in the complete set of folding curves found as Supplemental Figure 1. Not surprisingly, the speed of the reaction increased at higher concentrations of GSSG. For example, whereas 1SS and 2SS species dominate the folding mixture after 4–6 h at GSH/GSSG concentrations of 2/0 m*M* and are still found after 24 h of incubation, all peptides have been converted into 3SS species in GSH/GSSG 2/2 m*M* after only 1 h, as shown in Figure 2A and B. However, a significant proportion of these 3SS species were nonnative peptides, as judged from their LC-MS retention times, in folding buffers that did not contain iPrOH. In particular, nonnative 3SS species were the dominant species early in the reaction at 2/1 and 2/2 m*M* GSH/GSSG. However, in the presence of iPrOH (Fig. 2C and D) the level of such nonnative 3SS species decreased. As exemplified in Figure 2D, the route to N seems to bypass the accumulation of nonnative 3SS species in the presence of iPrOH, because of either a rapid conversion of these 3SS species to N, or a direct route from 2SS to N. This observation is consistent with the hypothesis that the hydrophobic fold of N is stabilized in the presence of organic solvent (13). In fact, iPrOH also stabilizes 2SS species that have native-like overall folds, as exemplified by the 2SS kinetic trap identified in (10); in the present study, the stable 2SS isomer contributes to the prolonged lifetime of 2SS species as shown in Figure 2C. Using only GSSG, the folding rate was increased even further (see graphs in Supplemental Fig. 1).

Importantly, the ability of iPrOH to stabilize N also helps in preventing deamidation of native kalata B1. Kalata B1 contains an Asn-Gly sequence that is surface/solvent exposed (consistent with it being the site of backbone cyclization), which might be prone to deamidation by formation of aspartimide followed by ring opening to Asp and iso-Asp, as

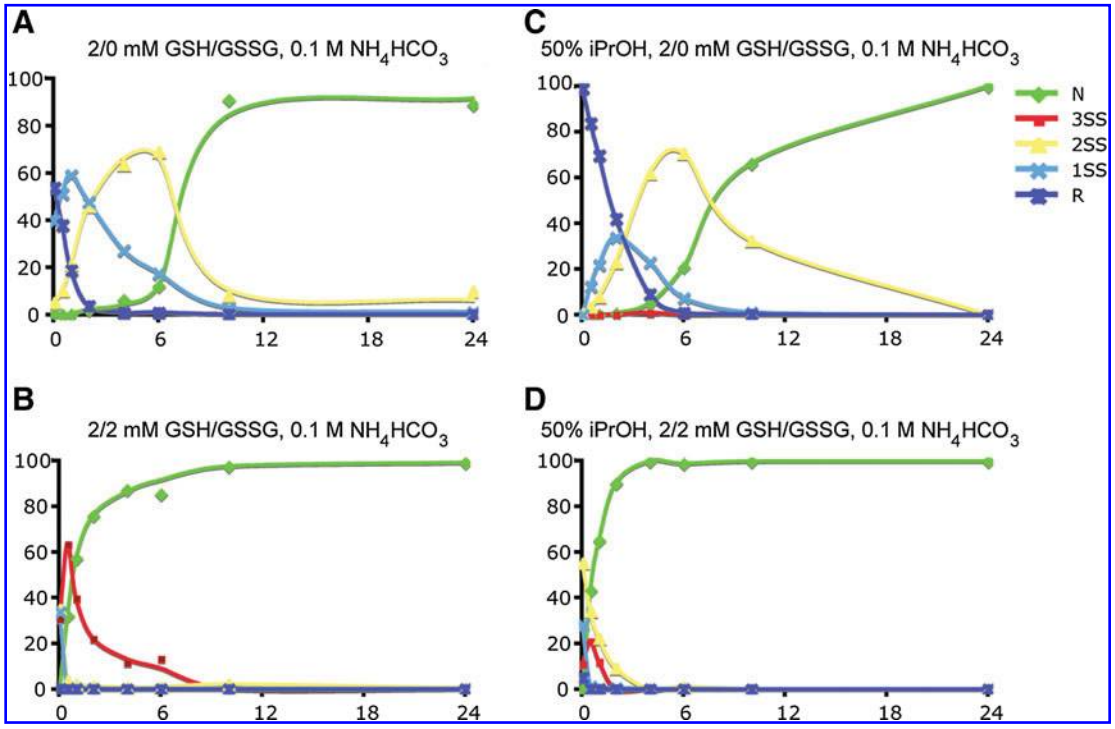

FIG. 2. Folding of kalata B1. (**A**) Reduced kalata B1 (R) in 0.1 *M* NH_4HCO_3 and 2 m*M* reduced glutathione (GSH) folds slowly *via* partly reduced species (peptide containing one disulfide bond [1SS] and peptide containing two disulfide bonds [2SS]). (**B**) Adding 2 m*M* oxidized glutathione (GSSG) makes folding much faster and *via* nonnative species with all cysteines oxidized (peptide containing three disulfide bonds [3SS]). (**C**) Adding the organic solvents isopropanol (iPrOH) also increases folding speed but not *via* 3SS derivates. (**D**) Folding in the presence of both GSSG and iPrOH oxidizes kalata B1 into native fold within a few hours. (Graphs of all folding experiments are provided as Supplemental Fig 1.)

depicted in Figure 3A. A detailed mapping using shallow gradient LC and offline MS, together with MS/MS analyses, shows that the latter two derivatives are significant side products in reactions done in ammonium bicarbonate buffer lacking iPrOH after extended incubation times (>72 h). The two peaks eluting immediately after the native peptide in Figure 3B had a mass increase of 1 mass unit compared with N. The position of the mass increase was localized to the Asn residue by MS/MS (data not shown). This observation is consistent with the conversion of Asn to Asp/iso-Asp. Strikingly, these derivatives constitute the main products at some conditions when folding rates are slow (*e.g.*, at GSH/GSSG 2/0 m*M*) and in the absence of iPrOH. Besides demonstrating an obvious stabilizing effect of iPrOH, these data suggest that deamidation occurs at all stages when the peptide is flexible in solution, including 3SS species that are in equilibrium with N.

Having established the influence of redox agents for the folding of kalata B1, 2/2 m*M* GSH/GSSG were chosen as standard concentrations for the folding experiments with the Möbius kalata B2, the bracelet cycloviolacin O2, and the hybrid kalata B8. In addition, the oxidative folding system recently developed specifically for the bracelet cyclotide cycloviolacin O2 (29) and a DMSO-based redox system were included (41). Specifically these buffers comprise 0.1 *M* Tris-HCl (pH 8.5) containing 1 m*M* EDTA, 6% Brij 35, 35% DMSO, and 2 m*M* cystamine, 2 m*M* GSH as redox agent, 20% DMSO, and 0.1 *M* ammonium bicarbonate.

The full set of graphs of those experiments can be found in Supplemental Figures 2–5; Figure 4, however, summarizes the folding efficiency of the different buffers, in terms of yield of N after selected time points of 30 min, 2 h, 6 h, and 24 h. The main difference between the three subfamilies is that the bracelet type is less prone to fold into the native structure, confirming earlier observations (20, 29). The yields of the Möbius cyclotides, kalata B1 and B2, and the hybrid kalata B8 all reach ~80% (or more) at some stage in some buffers, whereas the yield of the bracelet prototype reached a maximum of ~23% in the optimized buffer developed especially for that peptide. In other buffers used, the yield of native cycloviolacin O2 is negligible.

A closer examination of the yields shows that the two Möbius cyclotides follow the same folding pattern in the different buffers. The ammonium bicarbonate buffers with and without iPrOH result in good yields over 24 h and so does the buffer specifically designed for the bracelet cycloviolacin O2. However, the DMSO-containing ammonium bicarbonate buffer only gives N in yields of 10% and 16% for kalata B1 and B2, respectively, after 24 h. The levels of R, 1SS, or 2SS are negligible at any time point longer than 1 h for these cyclotides, with the exception of the 20% DMSO buffer, in which 2SS species are found at high levels up to 4 h. Noteworthy is also the equilibrium that is established between N and other 3SS species, which means that the yield of N does not increase at longer incubation times. These facts are clearly demonstrated by the folding curves found in Supplemental Figures 2–5, and exemplified by the folding curves for kalata B2 and cycloviolacin O2 in Figure 5, in which the equilibrium is established at a very low level of N. The folding of kalata B8 follows the same trends as the Möbius cyclotides, although the final yield is lower in most buffers.

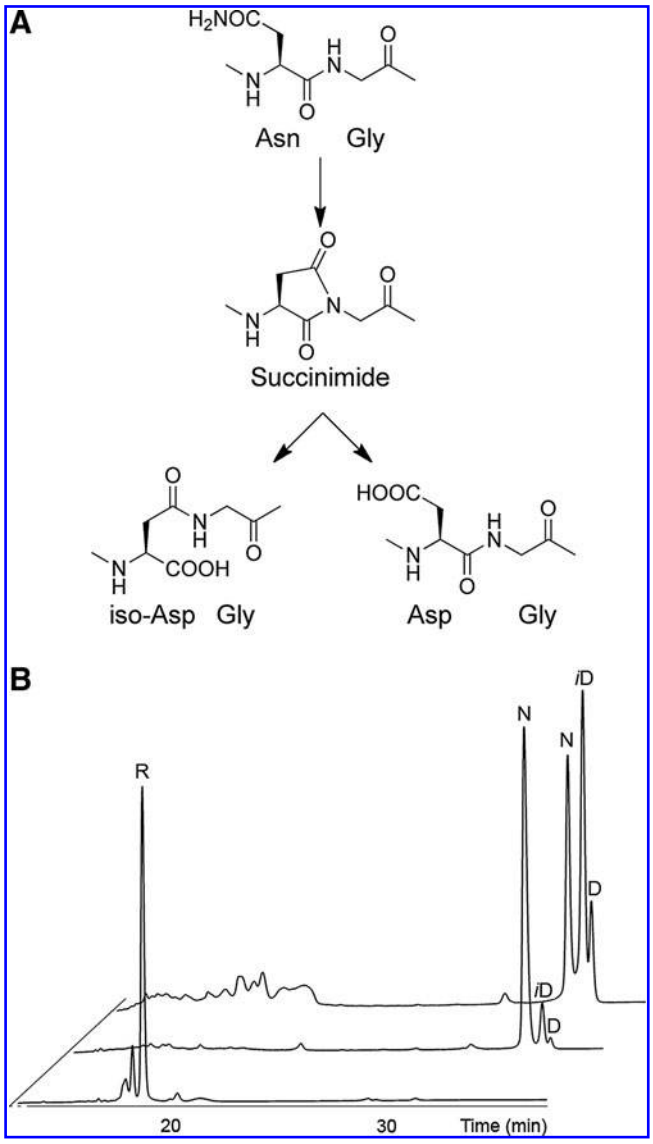

FIG. 3. Deamidation of kalata B1. Peptides, such as kalata B1, containing Asn-Gly sequences are particularly sensitive to deamidation, that is, the conversion of Asn to Asp and *i*-Asp as outlined in **A**. This reaction occurs spontaneously in solution at neutral pH. (**B**) The effects of that reaction after prolonged exposure in ammonium bicarbonate (pH 7.8), 2 m*M* GSH folding buffers with and without 50% iPrOH. The trace at the bottom shows the folding progress after 30 s: the reduced peptide (R, eluting at ~18 min) dominates in both buffers. The middle trace shows the folding after 72 h in the buffer containing iPrOH: N is the dominating product, but the two deamidation products emerge immediately after peptide with native disulfides (N) (*i*-Asp, *i*D; Asp, D). The upper trace shows the products in the buffer without iPrOH at the same time point; here the *i*-Asp derivative is the main product. Note the cluster of peaks occurring around 20 min in that trace: these are all 3SS products. Most likely these 3SS species are more susceptible to deamidation. The analyses were done using a Grom-Sil ODS-4 HE (125×2 [i.d.] mm, 3μm, 200 Å) column eluted with the following gradient from A (0.05% TFA in water [v/v]) to B (90% AcN in 0.045% TFA) at a flow rate of 0.3 ml/min: 0–5 min, 10% B; 5–10 min, 10%–27% B; 10–40 min, 27%–42% B; 40–45 min, 42%–100% B; 45–49 min, 100% B; 49–50 min, 100%–10% B.

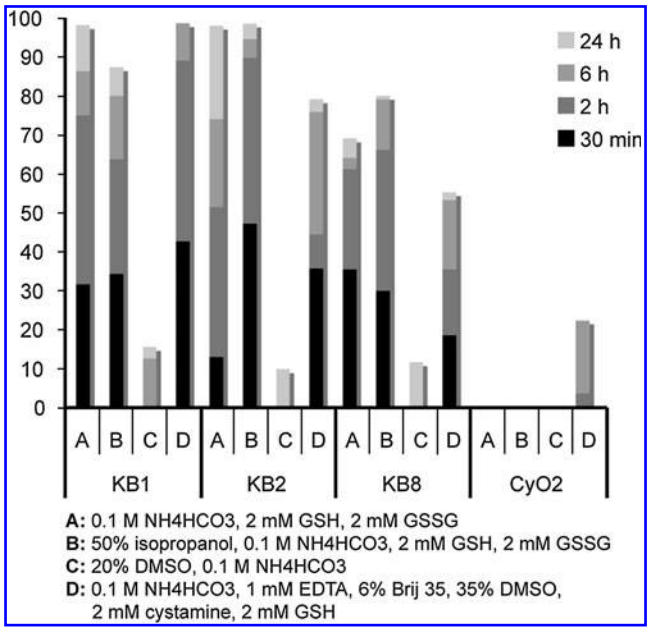

FIG. 4. Kinetics and yield of native cyclotide cyclotides in various buffers. Fully reduced kalata B1, B2, B8, and cycloviolacin O2 (KB1, KB2, KB8, and CyO2, respectively) were folded in four different buffers. Yields of native folds are shown as columns at four time points (30 min, 2 h, 6 h, and 24 h). The Möbius cyclotides KB1 and KB2 were possible to fold in all buffers but with low yields in the dimethyl sulfoxide (DMSO)-based system. The hybrid KB8 showed a similar pattern but with a lower final yield overall. The bracelet cyclotide CyO2 folded into N only in the buffer especially optimized for that cyclotide (at a yield of 23%).

Discussion

Developing an understanding of the pathway to formation of the topologically intriguing CCK motif, *in vivo* and *in vitro*, has been a major aim since the discovery and characterization of the first cyclotides. Aside from the fundamental interest in such novel protein topologies, there are practical benefits in understanding their folding pathways. For example, although approximately two-thirds of cyclotides belong to the bracelet subgroup, an understanding of the structure/function relationships of these peptides is relatively limited because of poor yields during oxidative folding and hence a lack of chemical mutagenesis studies. There is also significant interest in using cyclotides as scaffolds for grafting of bioactive peptide epitopes to produce stabilized peptide-based drug leads (5, 21, 43). However, advances in this area have, to some extent, been hampered by the lack of knowledge and approaches for the efficient folding *in vitro* of these reengineered cyclotides. The present study is the first attempt at a systematic evaluation of the oxidative folding, in terms of final yield and kinetics, of four protypical cyclotides.

The first part of the evaluation involved fine tuning of the redox system used, GSH and GSSG, which helps in the oxidation process by thiol/disulfide interchange. In these experiments, GSH concentration was kept constant, as the concentration of GSSG was varied. Not surprisingly, the results showed that the folding rate increased by decreasing the ratio of GSH/GSSG (*i.e.*, by decreasing GSH or increasing GSSG concentrations). This trend was the same in ammonium bicarbonate buffers with and without organic solvent. Incorporation of iPrOH into the folding buffer had a significant impact on the folding process for kalata B1. In ammonium bicarbonate buffer alone, folding was dominated by nonnative-like species, either 1SS or 2SS when GSSG was not present or 3SS species when GSSG was included. When iPrOH was added, more native-like folds were favored in the form of the stable 2SS intermediate identified previously (10) in the absence of GSSG or through the rapid formation of the native kalata B1 in the presence of GSSG. (The full set of folding curves is found as Supplemental Fig 1.)

We also observed that the folding rate, and thus indirectly the concentration ratio of redox agents, has a dramatic effect not only on the quantity of native peptide obtained but also on the degree of side reactions forming unwanted byproducts. Kalata B1, which was used as a model peptide in these initial experiments, contains an Asn-Gly sequence that was shown to be susceptible to conversion to Asp or iso-Asp *via* deamidation of Asn. This reaction is favored by a low degree of steric hindrance by the amino acid in the Asn+1 position and by conformational effects such as flexibility and solvent exposure. Both these conditions are fulfilled by kalata B1 during the folding process: the residue following Asn is Gly, and although cyclotides are stable and rigid molecules during the folding process, they do exhibit a significant degree of flexibility in the absence of disulfide bonds. Indeed, even three-disulfide-bond species have been shown to be flexible in solution in an earlier study (29).

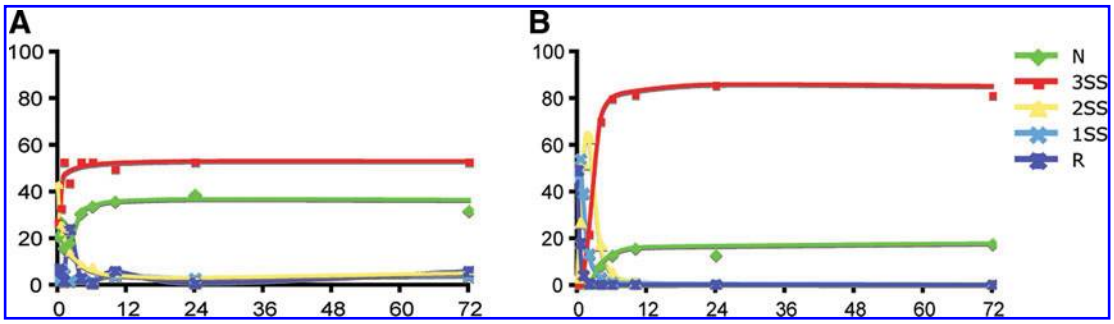

FIG. 5. Equilibriums are formed between N and 3SS species. Folding of cycloviolacin O2 gives low yield even in the folding buffer designed for that purpose: (**A**) Lower oxidation state products quickly disappear, followed by the establishment of an equilibrium between N and 3SS species. Kalata B2 shows a similar behavior in the 20% DMSO ammonium bicarbonate buffer (**B**); however, both 1SS and 3SS species are more long lived than in the case of **A**.

We were able to favor the formation of the deamidated derivatives by using conditions that induce slow folding (*i.e.*, the absence of GSSG and by using prolonged incubation times). At all sampled time points and at all tested concentrations of redox agents, however, the degree of deamidation significantly decreased if organic solvent (*i.e.*, iPrOH) was included in the folding buffer. This result is probably due to a stabilizing effect of the hydrophobic surface of the correctly folded cyclotide. This hypothesis is supported by the fact that the relative amount of kalata B1-folding products that have nonnative 3SS conformations is significantly lower in the presence of iPrOH, as shown by the HPLC analyses in Figure 3. Hypothetically, deamidation is a continuous reaction when the peptide occurs as these species, as they are more flexible than the native fold.

It is clear from these studies that choosing and keeping redox conditions under control is a key to a high-quality product. Our results also show the possible effects of storing cyclotides in solutions, which might favor reshuffling of disulfides and thereby promote flexibility and subsequent deamidation. The problem likely extends to other cyclotides, particularly when considering that the Asn-Gly sequence is present in most cyclotides, as it is the putative site of cyclization [other cyclotides contain Asp-Gly, which may be converted into iso-Asp but by a much lower degree (11)]. Of the other cyclotides studied in the present work, only cycloviolacin O2 contains Asn-Gly; we have not yet been able to detect any deamidated derivative of that peptide, most likely because it only folds in the specifically designed buffer that provides a highly stable environment for N.

We then turned to the folding evaluation of the four prototypic cyclotides: kalata B1 and B2 from the Möbius subfamily, cycloviolacin O2 from the bracelets, and the hybrid cyclotide kalata B8, which shares structural features from both the Möbius and bracelet subfamilies. Progress of the folding was followed over time in four different folding systems, and the ratios of R, 1SS, 2SS, 3SS, and N were calculated. All folding systems have been previously proven for some cyclotides: the ammonium bicarbonate buffers with and without iPrOH have been the standard buffers for most cyclotides syntheses (13, 38), albeit in the present experiments we used the optimized concentration of redox agents; the 20% DMSO is similar to the conditions used by Tam and coworkers for two-disulfide formation in a directed disulfide formation strategy for cyclotide synthesis (42); and finally, the rather complex buffer that was developed for the first direct folding of a bracelet cyclotide (cycloviolacin O2) (29).

These folding experiments confirmed that the *in vitro* oxidative folding of cyclotides can be very efficient in optimal conditions. There are some interesting aspects to the folding experiments, some unique to the individual examples used in the present study, with respect to the speed and efficiency of the disulfide bond formation. For the prototypical Möbius cyclotide, kalata B1, it was observed that the folding rate was slightly higher in ammonium bicarbonate buffer alone compared with when iPrOH was included in the system. For kalata B2, the second Möbius cyclotide studied, and the hybrid kalata B8, the opposite trend was observed, with the addition of iPrOH accelerating the folding. None of the tested cyclotides exhibited significant folding to the native isomer in the DMSO buffer. The bracelet cyclotide, cycloviolacin O2, only folded to the native isomer in the cycloviolacin O2-folding buffer as previously described (29). Interestingly, this oxidation buffer also produced native peptide for the other three cyclotides.

Although the Möbius cyclotides essentially follow the same folding pattern in terms of rate and yield of N, and also of the production of the 1SS and 2SS families of disulfide species, they differ significantly from the hybrid and bracelet cyclotides at the tested folding conditions (*c.f.* Fig. 5). An examination of the structures of these cyclotides helps in explaining these observations. Although the structures of the backbone and the overall sizes of the molecules are similar (*i.e.*, they all share the CCK motif), there are major differences when focusing on the properties of surface-exposed amino acid residues, as shown in Figure 6, particularly with respect to the degree and position of hydrophobic and charged residues. Although primarily residues in loops 5 and 6 form a hydrophobic patch in the two Möbius cyclotides, kalata B1

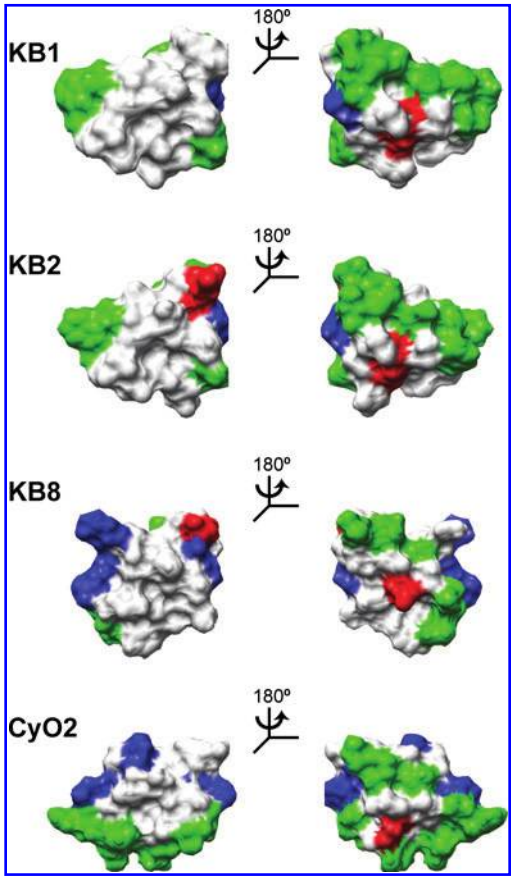

FIG. 6. Surface representations of aligned kalata B1, B2, B8, and cycloviolacin O2. In the Möbius cyclotides, kalata B1 and B2, the residues of loops 5 and 6, form a large hydrophobic patch, whereas in the bracelet cycloviolacin O2 the hydrophobic patch is comprised of residues from loops 2 and 3. The hybrid kalata B8 that consist of loops typical from both subfamilies lacks a well-defined hydrophobic patch. The hydrophobic patch of the cyclotides has a major influence on activity as well as the folding of the peptide. The hydrophobic residues (Ala, Leu, Ile, Pro Trp, Phe, and Val) are in green, cationic residues (Arg and Lys) in blue, anionic residues (Asp and Glu) in red, and other residues in white. (For interpretation of the references to color in this figure legend, the reader is referred to the web version of this article at www.liebertonline.com/ars).

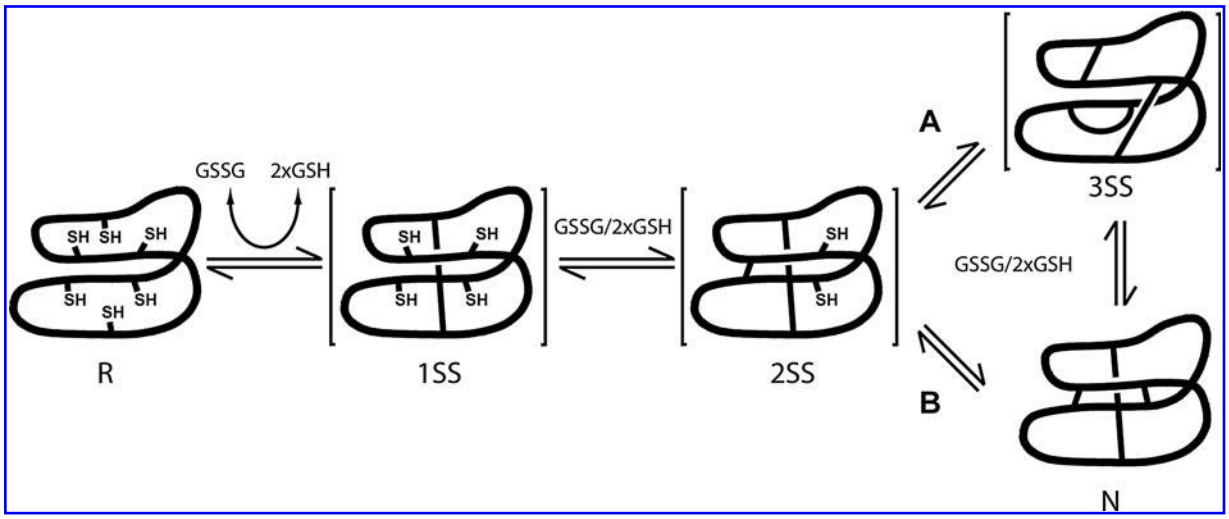

FIG. 7. Overview of folding pathway of cyclotides. Fully reduced cyclotides are folded *via* the partly oxidized species (1SS and 2SS) to the native structure. Some folding buffers seem to favor nonnative 3SS conformations that can directly flip to the native fold or go back through partly reduced species and then to the native structure. Path A is mainly and path B is partly favored in the folding pathway of Möbius cyclotides, whereas path B is the dominant folding pathway in the folding of bracelet cyclotides.

and B2, this region of the molecule is hydrophilic and charged in the bracelet cycloviolacin O2. On the contrary, cycloviolacin O2 displays a large hydrophobic patch centered around loop 2 and the α-helix in loop 3; the corresponding part of Möbius cyclotides is hydrophilic in nature. In comparison, kalata B8 has a relatively hydrophilic surface, lacking large hydrophobic surface patches. It has recently been shown that the location of these hydrophobic patches determines the mode of interaction with model membranes (37, 46). Hypothetically, these results can also be extended to their different folding behavior: the more amphipathic structure of cycloviolacin O2 requires not only a hydrophobic cosolvent but also a detergent for stabilization of the native form.

Although a good yield of N is the main purpose for most folding experiments, the demonstrated possibility to push equilibria to nonnative 3SS species, or to trap disulfide species of lower oxidation states by using slow or low-yielding folding systems, is potentially a valuable step toward a detailed understanding of the formation of the CCK motif. Currently, only one intermediate has been identified on the folding pathway of kalata B1, the most studied cyclotide. That 2SS species, shown in Figure 7, acts as kinetic trap (10) and is a major contributing factor to the high level of 2SS species in the iPrOH-containing buffer as shown by the folding curves in Figure 2. Using buffers that stabilize intermediates, for example, 20% DMSO/ammonium bicarbonate, could facilitate the isolation and identification of additional intermediates to provide a detailed map of the route to N.

Comparing the subsets of folding products and kinetics between the cyclotides in the present study reveals that the different subfamilies seem to follow two different routes to N, as outlined in Figure 7. The Möbius and hybrid cyclotides show 1SS/2SS species that are converted into N over a relatively long time span, whereas partially reduced (*i.e.*, 2SS) bracelet cycloviolacin O2 quickly collapses into nonnative 3SS species during oxidative folding. This is demonstrated in the folding curves found as Supplemental Figures 2–5: for example, the oxidation of cycloviolacin O2 2SS species in ammonium bicarbonate are effectively trapped as nonnative 3SS species, and only trace amounts of the lower oxidation forms (1SS/2SS) could be detected in the buffer designed for bracelets after 2 min. This suggests that Möbius/hybrids follow a 2SS to N route, whereas bracelets follow a pathway in which N is formed *via* concerted reshuffling of 3SS species. Alternatively, they all follow the same pathway, but their corresponding 3SS species are/is less stable; in that case a 3SS species could be the elusive direct precursor of N in all cyclotides. In this context it is noteworthy that the nonnative 3SS species depicted in Figure 7 has been recently identified as a major intermediate during the folding of cycloviolacin O2 and a synthetic Möbius/bracelet mutant (20, 29).

To date, a magic recipe has yet to be formulated that can be applied to the folding of all cyclotides. The need for such a recipe remains important as their stability and sequence diversity makes cyclotides attractive options as scaffolds for drug design. Their CCK motif has been shown to be essential for their exceptional stability, and therefore, it is vital that folding conditions are chosen for grafted analogs that generate molecules with a native fold. Cyclotides show promise as bearers of bioactive sequence epitopes, but even if there are some successful examples of active cyclotide analogs (21, 43), many of the trial-and-error peptides made in the course of these studies do not fold into cyclotide-like molecules. The results in the present study demonstrate that a plausible way to efficient folding is the development of a focused set of screening conditions, analogous to those used for screening crystallization conditions for X-ray studies (3). For that purpose, the buffer systems described here form a valuable starting point.

Acknowledgments

T.L.A. is supported by a grant from the Swedish International Development Cooperation Agency/The Department for Research Cooperation. R.J.C. is an NHMRC Career

Development Award Fellow. D.J.C. is an NHMRC Principal Research Fellow and is funded by the Australian Research Council. R.J.C. gratefully acknowledges the Australian Academy of Science for travel funding. U.G. is supported by the Swedish Research Council and the Swedish Foundation for Strategic Research.

Author Disclosure Statement

No competing financial interests exist.

References

1. Barbeta BL, Marshall AT, Gillon AD, Craik DJ, and Anderson MA. Plant cyclotides disrupt epithelial cells in the midgut of lepidopteran larvae. *Proc Natl Acad Sci U S A* 105: 1221–1225, 2008.
2. Barry DG, Daly NL, Bokesch HR, Gustafson KR, and Craik DJ. Solution structure of the cyclotide palicourein: implications for the development of a pharmaceutical framework. *Structure* 12: 85–94, 2004.
3. Chayen NE and Saridakis E. Protein crystallization: from purified protein to diffraction-quality crystal. *Nat Methods* 5: 147–153, 2008.
4. Clark RJ, Daly NL, and Craik DJ. Structural plasticity of the cyclic-cystine-knot framework: implications for biological activity and drug design. *Biochem J* 394: 85–93, 2006.
5. Craik DJ, Clark RJ, and Daly NL. Potential therapeutic applications of the cyclotides and related cystine knot miniproteins. *Expert Opin Investig Drugs* 16: 595–604, 2007.
6. Craik DJ, Daly NL, Bond T, and Waine C. Plant cyclotides: a unique family of cyclic and knotted proteins that defines the cyclic cystine knot structural motif. *J Mol Biol* 294: 1327–1336, 1999.
7. Craik DJ, Daly NL, Mulvenna J, Plan MR, and Trabi M. Discovery, structure and biological activities of the cyclotides. *Curr Protein Pept Sci* 5: 297–315, 2004.
8. Craik DJ, Simonsen S, and Daly NL. The cyclotides: novel macrocyclic peptides as scaffolds in drug design. *Curr Opin Drug Discov Devel* 5: 251–260, 2002.
9. Daly N, Clark R, Göransson U, and Craik D. Diversity in the disulfide folding pathways of cystine knot peptides. *Lett Pept Sci* 10: 523–531, 2003.
10. Daly NL, Clark RJ, and Craik DJ. Disulfide folding pathways of cystine knot proteins. Tying the knot within the circular backbone of the cyclotides. *J Biol Chem* 278: 6314–6322, 2003.
11. Daly NL, Clark RJ, Plan MR, and Craik DJ. Kalata B8, a novel antiviral circular protein, exhibits conformational flexibility in the cystine knot motif. *Biochem J* 393: 619–626, 2006.
12. Daly NL, Koltay A, Gustafson KR, Boyd MR, Casas-Finet JR, and Craik DJ. Solution structure by NMR of circulin A: a macrocyclic knotted peptide having anti-HIV activity. *J Mol Biol* 285: 333–345, 1999.
13. Daly NL, Love S, Alewood PF, and Craik DJ. Chemical synthesis and folding pathways of large cyclic polypeptides: studies of the cystine knot polypeptide kalata B1. *Biochemistry* 38: 10606–10614, 1999.
14. Dawson PE, Muir TW, Clark-Lewis I, and Kent SB. Synthesis of proteins by native chemical ligation. *Science* 266: 776–779, 1994.
15. Gillon AD, Saska I, Jennings CV, Guarino RF, Craik DJ, and Anderson MA. Biosynthesis of circular proteins in plants. *Plant J* 53: 505–515, 2008.
16. Göransson U, Herrmann A, Burman R, Haugaard-Jonsson LM, and Rosengren KJ. The conserved glu in the cyclotide cycloviolacin O2 has a key structural role. *Chembiochem* 10: 2354–2360, 2009.
17. Göransson U, Sjögren M, Svangård E, Claeson P, and Bohlin L. Reversible antifouling effect of the cyclotide cycloviolacin O2 against barnacles. *J Nat Prod* 67: 1287–1290, 2004.
18. Gran L. Oxytocic principles of *Oldenlandia affinis*. *Lloydia* 36: 174–178, 1973.
19. Gran L, Sandberg F, and Sletten K. *Oldenlandia affinis* (R&S) DC—a plant containing uteroactive peptides used in African traditional medicine. *J Ethnopharmacol* 70: 197–203, 2000.
20. Gunasekera S, Daly N, Clark R, and Craik DJ. Dissecting the oxidative folding of circular cystine knot miniproteins. *Antioxid Redox Signal* 11: 971–980, 2008.
21. Gunasekera S, Foley FM, Clark RJ, Sando L, Fabri LJ, Craik DJ, and Daly NL. Engineering stabilized vascular endothelial growth factor-A antagonists: synthesis, structural characterization, and bioactivity of grafted analogues of cyclotides. *J Med Chem* 51: 7697–7704, 2008.
22. Gustafson KR, Sowder RC, II, Henderson LE, Parsons IC, Kashman Y, Cardellina JH, II, McMahon JB, Buckheit RW, Pannell LK, and Boyd MR. Circulins A and B: novel HIV-inhibitory macrocyclic peptides from the tropical tree *Chassalia parvifolia*. *J Am Chem Soc* 116: 9337–9338, 1994.
23. Hernandez JF, Gagnon J, Chiche L, Nguyen TM, Andrieu JP, Heitz A, Hong TT, Pham TTC, and Nguyen DL. Squash trypsin inhibitors from *Momordica cochinchinensis* exhibit an atypical macrocyclic structure. *Biochemistry* 39: 5722–5730, 2000.
24. Herrmann A, Burman R, Mylne JS, Karlsson G, Gullbo J, Craik DJ, Clark RJ, and Göransson U. The alpine violet, *Viola biflora*, is a rich source of cyclotides with potent cytotoxicity. *Phytochemistry* 69: 939–952, 2008.
25. Ireland DC, Wang CK, Wilson JA, Gustafson KR, and Craik DJ. Cyclotides as natural anti-HIV agents. *Biopolymers* 90: 51–60, 2008.
26. Jennings C, West J, Waine C, Craik DJ, and Anderson M. Biosynthesis and insecticidal properties of plant cyclotides: the cyclic knotted proteins from *Oldenlandia affinis*. *Proc Natl Acad Sci U S A* 98: 10614–10619, 2001.
27. Jennings CV, Rosengren KJ, Daly NL, Plan M, Stevens J, Scanlon MJ, Waine C, Norman DG, Anderson MA, and Craik DJ. Isolation, solution structure, and insecticidal activity of kalata B2, a circular protein with a twist: do Mobius strips exist in nature? *Biochemistry* 44: 851–860, 2005.
28. Kamimori H, Hall K, Craik D, and Aguilar M. Studies on the membrane interactions of the cyclotides kalata B1 and kalata B6 on model membrane systems by surface plasmon resonance. *Anal Biochem* 337: 149–153, 2005.
29. Leta Aboye T, Clark RJ, Craik DJ, and Göransson U. Ultrastable peptide scaffolds for protein engineering-synthesis and folding of the circular cystine knotted cyclotide cycloviolacin O2. *Chembiochem* 9: 103–113, 2008.
30. Lindholm P, Göransson U, Johansson S, Claeson P, Gullbo J, Larsson R, Bohlin L, and Backlund A. Cyclotides: a novel type of cytotoxic agents. *Mol Cancer Ther* 1: 365–369, 2002.
31. Mulvenna JP, Sando L, and Craik DJ. Processing of a 22 kDa precursor protein to produce the circular protein tricyclon A. *Structure* 13: 691–701, 2005.
32. Plan MR, Göransson U, Clark RJ, Daly NL, Colgrave ML, and Craik DJ. The cyclotide fingerprint in *Oldenlandia affinis*: elucidation of chemically modified, linear and novel macrocyclic peptides. *Chembiochem* 8: 1001–1011, 2007.

33. Plan MR, Saska I, Cagauan AG, and Craik DJ. Backbone cyclised peptides from plants show molluscicidal activity against the rice pest *Pomacea canaliculata* (golden apple snail). *J Agric Food Chem* 56: 5237–5241, 2008.
34. Rosengren KJ, Daly NL, Plan MR, Waine C, and Craik DJ. Twists, knots, and rings in proteins. Structural definition of the cyclotide framework. *J Biol Chem* 278: 8606–8616, 2003.
35. Saska I, Gillon AD, Hatsugai N, Dietzgen RG, Hara-Nishimura I, Anderson MA, and Craik DJ. An asparaginyl endopeptidase mediates *in vivo* protein backbone cyclization. *J Biol Chem* 282: 29721–29728, 2007.
36. Schöpke T, Hasan Agha MI, Kraft R, Otto A, and Hiller K. Hämolytisch aktive komponenten aus *Viola tricolor* L. und *Viola arvensis* Murray. *Sci Pharm* 61: 145–153, 1993.
37. Shenkarev ZO, Nadezhdin KD, Sobol VA, Sobol AG, Skjeldal L, and Arseniev AS. Conformation and mode of membrane interaction in cyclotides. Spatial structure of kalata B1 bound to a dodecylphosphocholine micelle. *FEBS J* 273: 2658–2672, 2006.
38. Simonsen SM, Daly NL, and Craik DJ. Capped acyclic permutants of the circular protein kalata B1. *FEBS Lett* 577: 399–402, 2004.
39. Svangård E, Burman R, Gunasekera S, Lövborg H, Gullbo J, and Göransson U. Mechanism of action of cytotoxic cyclotides: cycloviolacin O2 disrupts lipid membranes. *J Nat Prod* 70: 643–647, 2007.
40. Svangård E, Göransson U, Hocaoglu Z, Gullbo J, Larsson R, Claeson P, and Bohlin L. Cytotoxic cyclotides from *Viola tricolor*. *J Nat Prod* 67: 144–147, 2004.
41. Tam J, Wu C, Liu W, and Zhang J. Disulfide bond formation in peptides by dimethyl-sulfoxide—scope and applications *J Am Chem Soc* 113: 6657–6662, 1991.
42. Tam JP, Lu YA, Yang JL, and Chiu KW. An unusual structural motif of antimicrobial peptides containing end-to-end macrocycle and cystine-knot disulfides. *Proc Natl Acad Sci U S A* 96: 8913–8918, 1999.
43. Thongyoo P, Bonomelli C, Leatherbarrow RJ, and Tate EW. Potent inhibitors of beta-tryptase and human leukocyte elastase based on the MCoTI-II scaffold. *J Med Chem* 52: 6197–6200, 2009.
44. Thongyoo P, Tate EW, and Leatherbarrow RJ. Total synthesis of the macrocyclic cysteine knot microprotein MCoTI-II. *Chem Commun (Camb)*: 2848–2850, 2006.
45. Wang CK, Colgrave ML, Gustafson KR, Ireland DC, Göransson U, and Craik DJ. Anti-HIV cyclotides from the Chinese medicinal herb *Viola yedoensis*. *J Nat Prod* 71: 47–52, 2008.
46. Wang CK, Colgrave ML, Ireland DC, Kaas Q, and Craik DJ. Despite a conserved cystine knot motif, different cyclotides have different membrane binding modes. *Biophys J* 97: 1471–1481, 2009.
47. Wang CK, Hu SH, Martin JL, Sjögren T, Hajdu J, Bohlin L, Claeson P, Göransson U, Rosengren KJ, Tang J, Tan NH, and Craik DJ. Combined X-ray and NMR analysis of the stability of the cyclotide cystine knot fold that underpins its insecticidal activity and potential use as a drug scaffold. *J Biol Chem* 284: 10672–10683, 2009.
48. Witherup KM, Bogusky MJ, Anderson PS, Ramjit H, Ransom RW, Wood T, and Sardana M. Cyclopsychotride A, a biologically active, 31-residue cyclic peptide isolated from *Psychotria longipes*. *J Nat Prod* 57: 1619–1625, 1994.

Address correspondence to:
Dr. Ulf Göransson
Division of Pharmacognosy
Department of Medicinal Chemistry
Biomedical Centre
Uppsala University
Box 574
Uppsala SE 75123
Sweden

E-mail: ulf.goransson@fkog.uu.se

Date of first submission to ARS Central, January 25, 2010; date of final revised submission, April 21, 2010; date of acceptance, May 15, 2010.

Abbreviations Used

0SS = reduced peptide without disulfide bonds
1SS = peptide containing one disulfide bond
2SS = peptide containing two disulfide bonds
3SS = peptide containing three disulfide bonds
CCK = cyclic cystine knot
DMSO = dimethyl sulfoxide
EDTA = ethylenediaminetetraacetic acid
GSH = reduced glutathione
GSSG = oxidized glutathione
HPLC = high-performance liquid chromatography
iPrOH = isopropanol
LC = liquid chromatography
MS = mass spectrometry
N = peptide with native disulfides
N3SS = native peptide with three native disulfide bonds
NEM = *N*-ethylmaleimide
NN3SS = nonnative peptide fold containing three disulfide bonds
R = reduced peptide

This article has been cited by:

1. Hossein Hashempour, Johannes Koehbach, Norelle L. Daly, Alireza Ghassempour, Christian W. Gruber. 2012. Characterizing circular peptides in mixtures: sequence fragment assembly of cyclotides from a violet plant by MALDI-TOF/TOF mass spectrometry. *Amino Acids* . [CrossRef]
2. Ji-Shen Zheng, Shan Tang, Ye Guo, Hao-Nan Chang, Lei Liu. 2012. Synthesis of Cyclic Peptides and Cyclic Proteins via Ligation of Peptide Hydrazides. *ChemBioChem* n/a-n/a. [CrossRef]
3. Anne C. Conibear, David J. Craik. 2011. Chemical Synthesis of Naturally-Occurring Cyclic Mini-Proteins from Plants and Animals. *Israel Journal of Chemistry* n/a-n/a. [CrossRef]
4. W. Xu, L. Li, L. Du, N. Tan. 2011. Various mechanisms in cyclopeptide production from precursors synthesized independently of non-ribosomal peptide synthetases. *Acta Biochimica et Biophysica Sinica* . [CrossRef]
5. David J Craik, Anne C Conibear. 2011. The Chemistry of Cyclotides. *The Journal of Organic Chemistry* **76**:12, 4805-4817. [CrossRef]
6. David J. Craik . 2011. The Folding of Disulfide-Rich Proteins. *Antioxidants & Redox Signaling* **14**:1, 61-64. [Abstract] [Full Text HTML] [Full Text PDF] [Full Text PDF with Links]